JOURNAL OF MECHANICAL ENGINEERING AND SCIENCES (JMES)
ISSN: 2289-4659 e-ISSN: 2231-8380
VOL. 14, ISSUE 3, 7029 – 7039
DOI: https://doi.org/10.15282/jmes.14.3.2020.05.0550

ORIGINAL ARTICLE

Computational analysis to predict the effect of pre-bifurcation stenosis on the hemodynamics of the internal and external carotid arteries

H. Bouteloup[1], J.G.O Marinho[1,2], S. Chatpun[3,*] and D.M. Espino[1]

[1] Department of Mechanical Engineering, University of Birmingham, B15 2TT, United Kingdom
[2] Centro de Tecnologia e Geociências, Universidade Federal de Pernambuco, Cidade Universitária Recife, Recife, Brazil
[3] Institute of Biomedical Engineering, Faculty of Medicine, Prince of Songkla University, Hatyai, Songkhla 90110, Thailand
Phone: +66880891379

ABSTRACT – This study assessed the hemodynamics of a patient-specific multiple stenosed common carotid artery including its bifurcation into internal and external carotid arteries; ICA and ECA, respectively. A three-dimensional computational model of the common carotid artery was reconstructed using a process of segmentation. Computational fluid dynamics was applied with the assumption that blood is Newtonian and incompressible under pulsatile conditions through the stenotic artery and subsequent bifurcation. Blood was modelled as 'normal' and 'hyperglycaemic'. A region of large recirculation was found to form at bifurcation. The asymmetric velocity flow profile through the ICA was evident through the cardiac cycle with higher velocity at the inner walls of ICA. Hyperglycaemia was found to increase wall shear stresses on the carotid artery and reduce the blood velocity by as much as 4 times in ECA. In conclusion, hemodynamics in ICA and ECA are not equally affected by stenosis, with hyperglycaemic blood potentially providing additional complications to the clinical case.

ARTICLE HISTORY
Revised: 22nd May 2020
Accepted: 28th May 2020

KEYWORDS
Carotid artery; computational fluid dynamics; hemodynamics; magnetic resonance; patient-specific stenosis

INTRODUCTION

Cardiovascular disease is the major cause of mortality world-wide according to the World Health Organization [1]. Vascular atherosclerosis is a vascular wall thickening caused by atherosclerotic plaque which leads to a narrow lumen causing blood flow insufficiency. Vascular atherosclerosis can exist in several locations of the vascular network such as carotid arteries, cerebrovascular arteries, coronary arteries and aorta [2–5]. In terms of stenosis of carotid arteries, a specific risk is that of stroke due to insufficient blood supply to brain [6, 7]. Furthermore, vascular stenosis is associated with perturbed blood flow patterns and altered wall shear stress [8, 9]. Therefore, there has been much focus on understanding vascular plaque formation and predicting the effects of stenosis on hemodynamics [10–12]. One such approach is to use numerical models to calculate blood flow [13]. As blood flow through the circulatory system is pulsatile, computational studies use transient models [8, 14, 15]. Computational fluid dynamics (CFD) models in particular are useful because to study either static or transient blood flow, where three-dimensional models can be generated from medical images. Thus, CFD models enable a link between clinical scans and blood flow patterns as predicted for an individual, with the potential to assist in the assessment of any hemodynamic changes through the anatomically accurate geometries [14, 16, 17].

There has been a recent trend towards combining medical imaging technologies such as computer tomography (CT) [5, 18], echo-Doppler [19, 20] and magnetic resonance (MR) [8, 21] with computational modelling. Although it is feasible to reconstruct highly detailed images based on scans of ex vivo tissues [22], however, such techniques are currently limited in terms of clinical translation because the imaging modalities are not used in clinically. Thus, transformation of medical images to a computer-reconstructed geometry enables the generation of patient-specific models and subsequently predictions which can potentially aid clinicians in their evaluation of an individual. For example, Li et al. analysed flow patterns in a highly stenotic patient-specific carotid bifurcation model reconstructed from MR images [8]. The CFD study performed by Li et al. used a turbulence model, with the outcome that high wall shear stress (WSS) were induced along the inner wall of an internal carotid artery where a stenosis was presented. Further, there was a relatively low time-averaged WSS at the wall of the external carotid artery. Where stenosis is found along the human thoracic aorta, the maximum WSS appears to occur in the areas between left common carotid and left subclavian arteries; determined using a three-dimensional model of human thoracic aorta, with pulsatile blood flow, developed using CT images and CFD [5].

The bifurcation of the carotid arteries into an internal carotid artery (ICA) and external carotid artery (ECA) is of important clinically because of the changes in blood flow at a bifurcation of arteries which supply blood to the brain. Hence, the interest in the hemodynamics through bifurcations [23, 24], with the potential to map WSS on to medical scans. While idealized geometrical models have been useful in determining strategies best equipped to mimic blood rheology [10], and subject specific models have been used to model turbulence in a patient-specific post-bifurcation stenosis model [8], it is still necessary to investigate how pre-bifurcation stenosis affects parameters such as WSS and

*CORRESPONDING AUTHOR | S. Chatpun | ✉ surapong.c@psu.ac.th

flow patterns on an anatomical model of the bifurcating carotid artery. Moreover, given the clinical implications of changes to ICA and ECA flow during stenosis [8], it is necessary to assess how a pre-bifurcation stenosis might alter flow through both branching arteries. Clinically, though, patients may present with further complications for instance through changes in blood rheology. For example, pathological conditions (i.e. diabetes mellitus, sickle cell anemia) may affect blood rheology and impose additional complications to vascular stenosis [25–28]. Thus, assessing the sensitivity of model predictions to altered blood rheology is potentially of clinical value.

This study aimed to compare the downstream effect of multiple stenoses along a common carotid artery, using a patient-specific geometry, and evaluate changes to blood flow through both the ICA and ECA. A transient model with a non-hyperglycemic viscosity has been solved using CFD to compare flow through the ICA and ECA downstream of a stenosis, including analysis of wall shear stresses on inner and outer walls of the ICA. A steady state model has also been used to enable a simplified comparison between otherwise typical and hyperglycaemic blood rheology in this multiple stenosed model.

METHODS AND MATERIALS

Vascular Geometry Acquisition and Reconstruction

The carotid artery geometric data was acquired from a 66-year-old male patient who was diagnosed to have 38% of luminal narrowing and found to have multiple stenotic regions along the left carotid artery at the level of the throat. The carotid artery was imaged using a 3.0 T Magnetic Resonance scanner (Achieva 3.0 T X-series MRI system, Philips, The Netherland) with time of flight angiography. A total of 140 slices were obtained from the scanning sequence. Each image obtained had a slice thickness of 2.5 mm, with no gaps between image slices. The protocol of this acquisition was approved by the institutional ethics committee (EC-56-113-25-2-3). All procedures for the geometric data acquisition were performed at Songklanagarind hospital (Songkhla, Thailand), and informed consent was obtained from the patient. All procedures were in accordance with the 1964 Helsinki declaration. A scanned image of the patient's carotid artery is shown in Figure 1(a).

Segmentation software (Simpleware Scan IP, Simple-ware, Exeter, UK) was used to create a three-dimensional model of the carotid artery, including constriction and bifurcation (Fig. 1b). A threshold-based technique was used to identify different structures along the carotid artery. The blood visible from the MR Angiography (MRA) scan-data was reconstructed for each scan-slice with interpolation used between slices. Cavity fill and island removal tools were used to fill in voids so as to form a continuum of blood and to remove small isolated regions, presumed to be noise-artefacts, during the scan, respectively.

Computational Modelling

Blood rheological properties were assumed as incompressible and a Newtonian fluid. This is a valid assumption under large scale flow [29]. Blood was modelled to have a density of 1,050 kg/m^3 with a viscosity of 4 ×10-3 Pa·s[30, 31]. Hyperglycaemia was modelled by increasing the blood viscosity to 5×10^{-3} Pa·s [32].

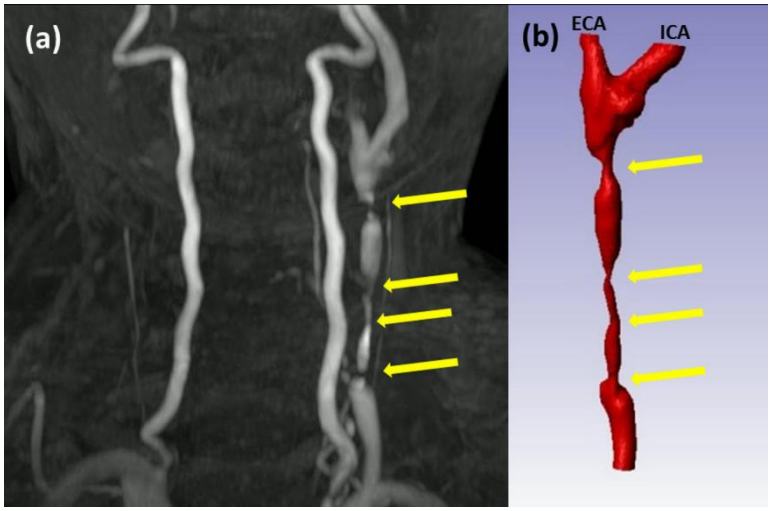

Figure 1. Patient-specific carotid artery (a) Magnetic resonance angiography of left carotid arteries, and (b) reconstructed geometry of carotid artery. Yellow arrows point to the stenosis sites

A combination of mass flow rate inlet and a pressure outlet were applied as boundary conditions, along with no-slip wall conditions on a rigid wall model of the carotid artery [33, 34]. Steady state models were run with an inlet speed of 0.3 m/s and with an outflow and a reference pressure of 70 mmHg [35]. For transient models, blood inflow was simply

modelled with a spatially uniform mass inflow rate, (g/s) entering through the distal boundary of the carotid artery model (Eq. (1); Figure 2a) [36]. The outlet at the inner and outer arteries was set to a time-dependent pressure, P (mmHg) at a given time, t (Eq. (2); Figure 2b). Transient simulations were set to run for 0.9 s, with a reference pressure of 70 mmHg [35].

$$\dot{m} = \begin{cases} 2+150t, t < 0.10 \\ 10-10.5t, t \geq 0.10 \end{cases} \quad (1)$$

$$P = 70 + 30\sin\left(\left(\frac{\pi}{3}\right)(t-0.05)/0.15\right) \quad (2)$$

Multiple meshed geometries were exported to assess mesh convergence and ensure that wall shear stresses and peak velocities predicted had converged to within 1% [16]. The model was meshed with tetrahedral elements and following mesh convergence the final mesh used for models had 937,086 elements.

The finite volume package, ANSYS CFX (v14.5, ANSYS Inc., Canonsburg, PA, USA) was used to solve the steady-state and transient CFD models. Fluid dynamics were solved using the continuity equation and incompressible Navier-Stokes equations. The assumption of a supine position was used, so that the body force term was omitted from the Navier-Stokes equations [37], and the κ-ε turbulence model was used as the peak Reynolds numbers were above that anticipated for laminar flow. The effect of laminar versus turbulent flow predictions in CFD models reconstructed from clinical scans has been presented elsewhere [13].

The velocity through the carotid artery was measured on the cross section of the ICA and ECA, along two faces but perpendicular axes termed first and second directions (approximately aligned with medial-lateral and anterior-posterior anatomical axes, respectively; Figure 3). This provides a normalized velocity flow profile along two perpendicular axes of the cross section of the blood vessel, where a value of 1 means that outflow through the artery matches the inflow to the artery distal to the stenosis or bifurcation. Furthermore, the velocity ratio was calculated from the peak value of the inlet velocity, u, and the velocity at specific points across both directions of the ICA, vICA, and ECA, vECA, using Eqs. (3) and (4), respectively [27].

$$V_{ICA} = \frac{v_{ICA}}{u} \quad (3)$$

$$V_{ECA} = \frac{v_{ECA}}{u} \quad (4)$$

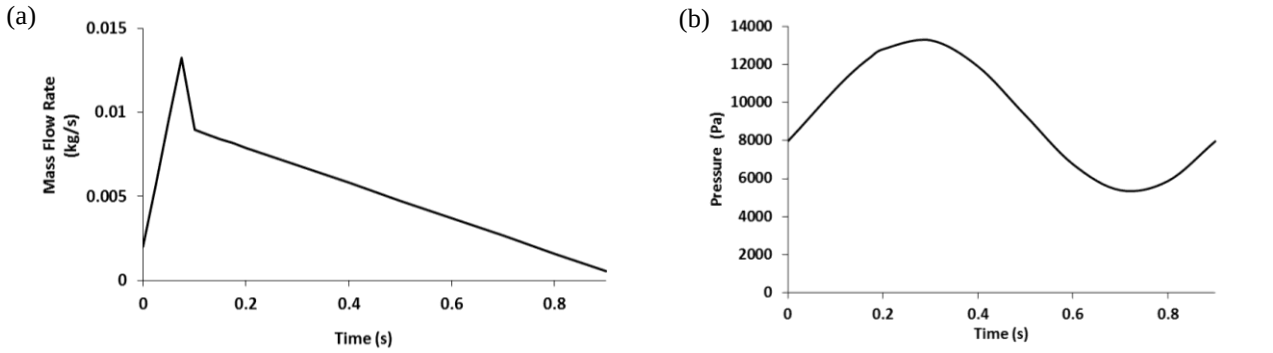

Figure 2. Transient boundary conditions: (a) mass flow rate, and (b) pressure outlet

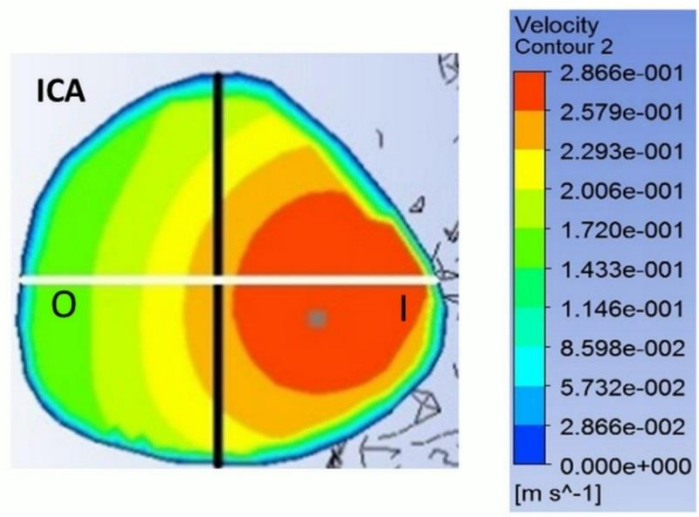

Figure 3. Velocity ratio measurement landmarks. The white line marks the first direction whereas the black line marks the second direction across which measurements were exported. I: inner wall; O: outer wall

RESULTS

Transient Flow

There was a large pressure drop and an increase in blood velocity across the narrowest diameter of the stenosed artery, approximately 4 cm from the bifurcation (Figure 4). At 0.075 s, the pressure dropped approximately 70 kPa (Figure 4a) and blood velocity increased up to 17 m/s (Figure 4b). After this region of stenosis there was a large area of recirculation (Figure 4b). These pressure drops correspond with the explanation using Bernoulli equation when flow passes through a narrowing conduit.

Transient peak velocity at the central point of the ECA and ICA outflow cross section occurred at 0.075 s, reaching 0.60 m/s for the ECA and 0.35 m/s for the ICA (Figure 5). From 0.1 s onwards, blood velocity was higher in the ICA than the ECA (Figure 5). There was a sharp drop in ECA velocity at around 0.1 s tending towards 0 m/s which remained at that order of magnitude throughout the rest of the blood flow cycle. Instead, flow through the ICA was more constant with the velocity decreasing from 0.30 m/s, at 0.2 s, to 0.20 m/s at 0.6 s and gradually tending towards 0 m/s.

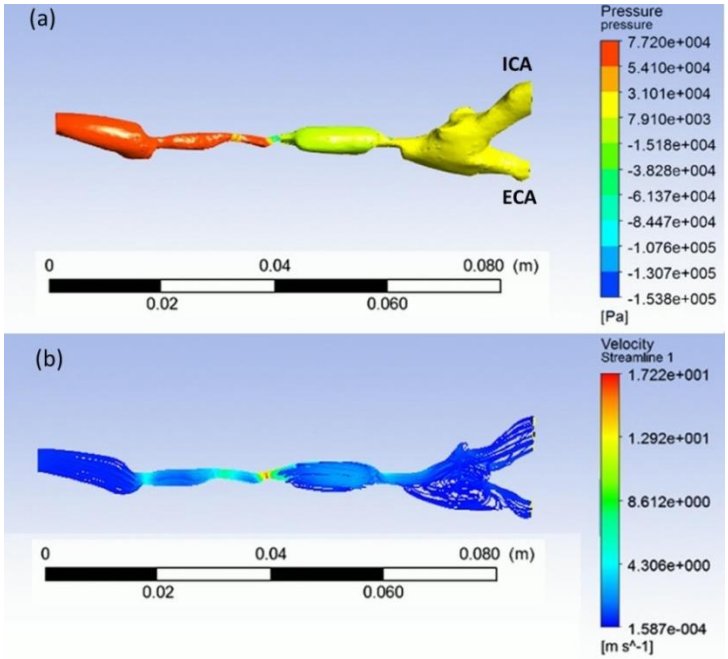

Figure 4. Flow through the carotid artery at 0.075 s (peak flow) including (a) pressure, and (b) flow velocity. ICA: internal carotid artery; ECA: external carotid artery

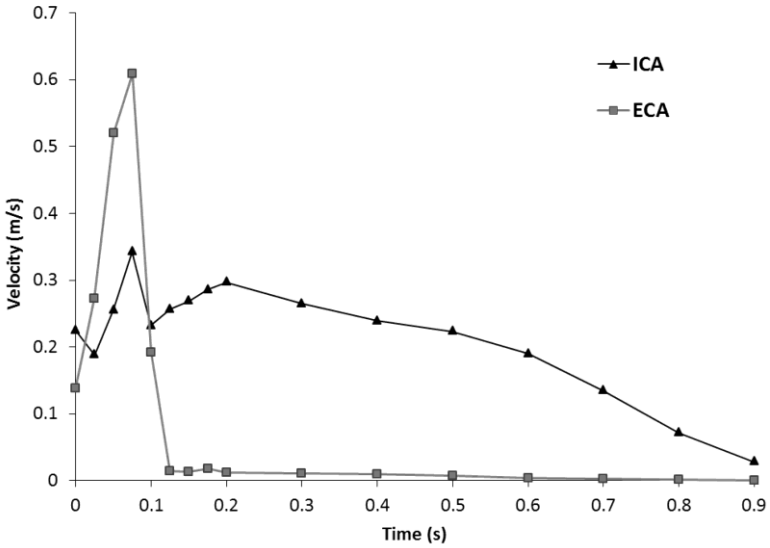

Figure 5. Outlet velocity in internal carotid artery (ICA) and external carotid artery (ECA) in a stenosed carotid artery using a transient flow model. Velocity was measured at a central point of the outflow cross section of each artery

An asymmetric velocity flow profile through the ICA was evident throughout the cardiac cycle with higher velocity at the inner walls of the ICA (Figure 6a and 6b). Although the central point of the cross section experienced a reduction in velocity throughout the blood-flow cycle, peak blood velocity of up to 0.64 m/s was evident towards the inner walls of the ICA at up to 0.8 s of the cycle. The asymmetric flow led to differences between the WSS at the inner and outer wall of the ICA (Figure 7). At 5 mm from the bifurcation, the WSS for the inner wall of the ICA peaked, at 0.1 s, at 4.5 Pa as compared to less than 2 Pa for the outer wall. This result follows the theoretical concept that the magnitude of WSS is proportional to the velocity gradient near the wall or the wall shear rate because at the inner wall of ICA had a higher velocity gradient than the outer wall of the ICA [38].

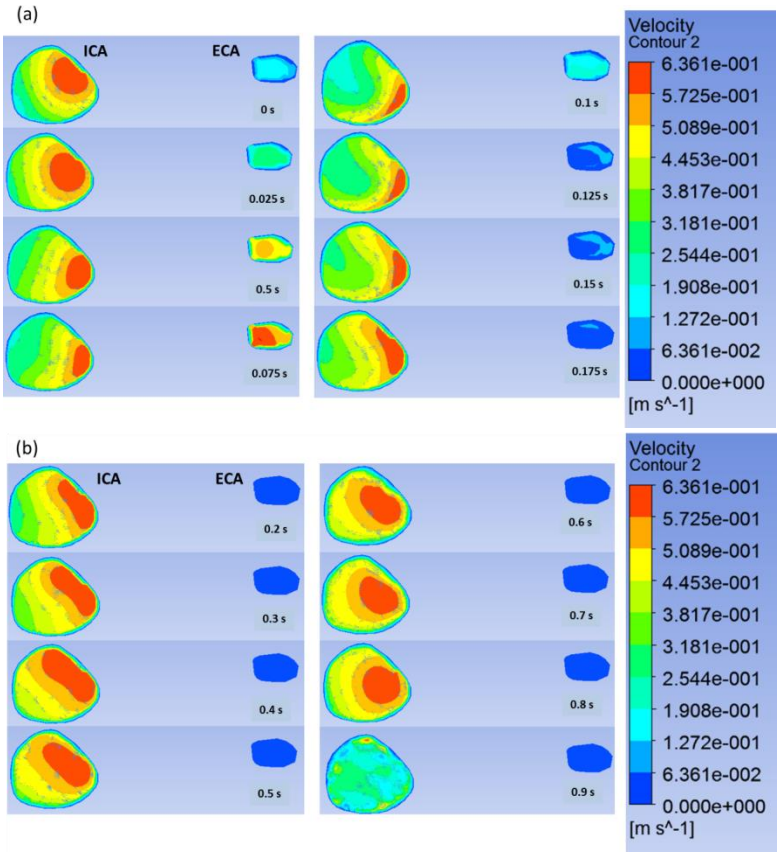

Figure 6. Outlet velocity contour at each specific time of simulation in a transient flow model. For time-steps: (a) 0 to 0.175 s and (b) 0.2 to 0.9 s. ICA: internal carotid artery; ECA: external carotid artery

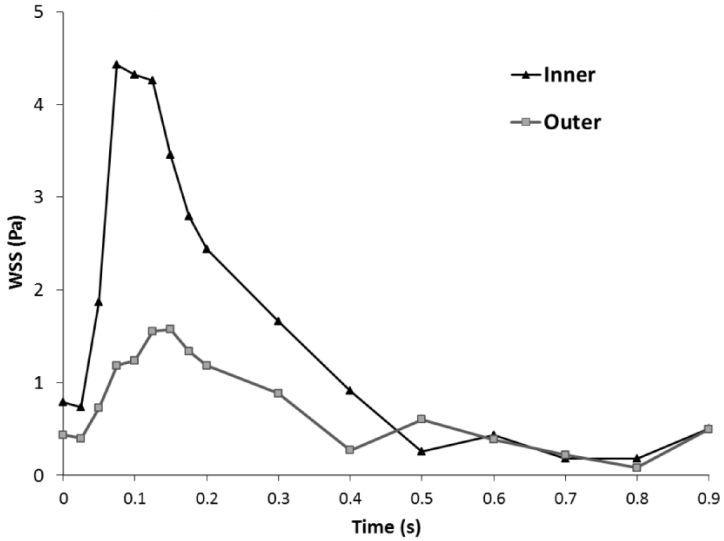

Figure 7. Wall shear stress (WSS) on the inner wall and outer wall of internal carotid artery at 5 mm from the bifurcation

Steady State Comparison of Normal and Hyperglycaemic Blood Viscosity

Figures 8(a) to 8(d) provide steady-state flow profiles along the first direction (Figure 8a and 8b); ICA and ECA, respectively) and second direction (Figure 8c and 8d; ICA and ECA, respectively) identified across the cross-sections of arteries. Hyperglycaemic blood led to a reduced velocity ratio in the ECA. At the centre of the ECA, the velocity ratio decreased from approximately 0.4, for 'normal blood', to approximately 0.1 (Figure 8b and 8d). However, the changes in the velocity ratio were less pronounced for the ICA (Figure 8a and 8c), typically differing by less than 0.1, with similar velocity flow profiles.

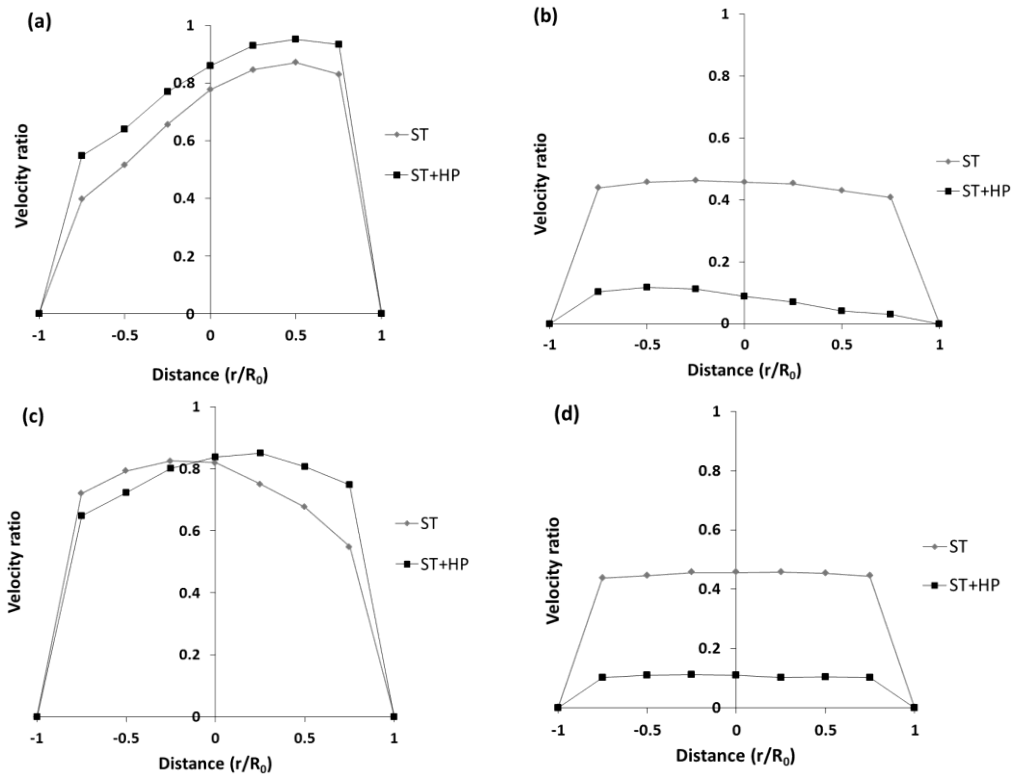

Figure 8. Steady-state velocity ratio in the first direction: (a) internal carotid artery and (b) external carotid artery. Velocity ratio in the second direction for (c) internal carotid artery and (d) external carotid artery. (a steady flow model; ST: stenosis, ST+HP: stenosis and hyperglycemia)

The non-symmetric flow profile along the ICA led to the differences in WSS between inner and outer walls of ICA. For normal viscosity, WSS decreased from 1.8 to 1.2 Pa along the inner wall (Figure 9a) but from 0.6 to 0.2 Pa along the outer wall of the ICA (Figure 9b). Hyperglycaemic blood increased wall shear stresses along the outer wall of the ICA but followed a similar trend of decreasing along the length of the arterial wall (ranging from 1.4 to 0.4 Pa; Figure 9b). However, hyperglycaemic blood led to an increase in WSS along the inner wall (increasing from 0.4 to 1.4 Pa along the wall; Figure 9a).

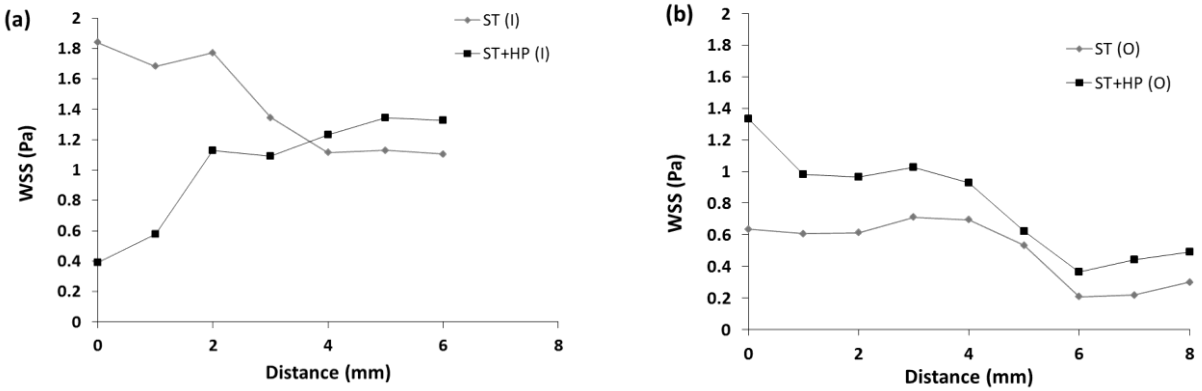

Figure 9. Steady-state wall shear stress (WSS) on the (a) inner wall and (b) outer wall of the internal carotid artery (ICA) cranial to the bifurcation. Note, ST denotes Stenosed; HP Hyperglycaemic; O and I outer and inner walls

DISCUSSION

This study demonstrates a proof of principle for clinical translation using a combination of clinical imaging and computational methods to study a three-dimensional computational fluid dynamics model of a patient-specific, multiple stenosed, carotid artery and bifurcation. The model was reconstructed following magnetic resonance angiography. This study highlights the need to evaluate numerical methods with current imaging modalities available clinically; this is so that CFD, in this case, can be used to inform clinical practice. The patient-specific CFD model predicted a pressure drop across the stenosis (not unexpectedly), and downstream of the stenosis predicted a large region of recirculating blood flow. There was also a difference in the blood flow velocity through the two bifurcating arteries, with an approximately symmetrical boundary layer through the ECA and with peak flow velocity occurring approximately at a centre point. However, for the ICA peak velocity occurred towards the inner wall of the artery with a corresponding increase in WSS. In this current study, hyperglycaemia typically increased the predicted WSS along arteries, and in addition led to a decrease in the velocity ratio by up to a factor of ×4.

There are a range of factors that affect the hemodynamics through the cardiovascular system. For example, vascular geometry, blood viscosity, the duration of the cardiac cycle (as well as the time at which the cardiac cycle is analysed), wall elasticity and any underlying pathological conditions. It has been demonstrated that the degree of stenosis influences the blood flow pattern, velocity, pressure and wall shear stress both at the level of the throat but also downstream of stenosis [5, 8, 12]. Indeed a severe blockage, such as an 82% grade of stenosis in the external carotid artery, can cause a large pressure drop across the throat and increased the velocity at the throat about ×2 as compared with a healthy model [2]. Furthermore, WSS was increased at the level of the throat, with the potential to damage endothelial cells. Our study looked at the velocity at the distal distance from the stenotic regions in the ICA and ECA; we found that velocities in both arteries decreased as compared to the inlet velocity. Further, in steady state models, our study showed that the velocity ratio at the ECA was reduced when the blood viscosity increased (this occurred along both the first and second direction measurements; Eqs. (3) and (4)). These velocity ratios can be useful for clinical pre-screening on luminal narrowing of the common carotid artery [39]. Thus, in our model, there is an increased risk of plaque formation in the ECA due to the lower WSS predicted.

Many recent studies have assessed pulsatile flow instead of the steady flow so as to mimic the natural pulse of the cardiovascular system. As a cardiac cycle includes systole and diastole, blood flow varies during this period leading to a change in velocity, pressure and WSS in the vasculature [7]. Systole corresponds to the peak velocity in a cardiac cycle. In addition, for aortic stenosis the maximum WSS presented at the peak systole in either symmetric or asymmetric stenosis [5]. It was also demonstrated by Lee et al., using transitional flow, that rapid velocity and pressure fluctuation presented in the post-stenotic region, as well as high WSS during systole [40]. The study in a highly stenotic patient-specific carotid bifurcation model revealed that the high time-averaged WSS was at the throat of stenosis and on the inner wall of ICA [8]. The order of magnitude of WSS in our study was in the same range as that reported by Markl et al. and Gharahi et al. [40, 41]. Furthermore, the high pressure drop across the carotid artery at the level of the throat occurred during peak systole. Similarly, our model predicted that high blood flow velocities presented towards the inner wall of ICA, which in turn led to the high WSS at the inner wall during the early systolic phase. Furthermore, our study found a region of recirculating blood immediately downstream from the stenosis, consistent with flow separation following stenosis [43],

this is relevant because it may be linked to atherosclerotic lesion development [44]. Using a transient analysis, it was found that eddies were forming downstream of the stenosis due to a pressure drop [17]. The patient studied in this present report had multiple stenoses along the carotid artery, consistent with this self-perpetuating model of an atherosclerotic lesion. Indeed plaque formation is caused by low shear stress inducing intimal thickening [9]. Long et al. simulated the pulsatile blood flow through arterial stenosis and found that WSS changed between negative and positive value downstream of the stenosis [45]. Therefore, existing studies and our present study emphasize that transient blood flow models provide useful insight as to high and low WSS during a cardiac cycle.

As with any study, there are several limitations to this study. First, there were some artefacts in the MR image of the patient which resulted in an incomplete carotid artery geometry reconstruction. This required the use of a cavity filling when reconstructing the geometry. This issue is common to segmentation. Second, our model used a linearized waveform of mass flow rate. This waveform could give us a picture of blood flow including hemodynamic changes downstream from the multiple stenoses and carotid bifurcation. However, it is feasible to add a patient specific waveform for more specific understanding to a given individual [19, 20, 46]. Third, physiologically, blood pressure is pulsatile with dependency on both the pumping of the heart and also vascular compliance; which can be characterised using elastic (linear or non-linear) and viscoelastic properties [47, 48]. However, this compliance was not accounted for in our models. In addition, patient-specific boundary conditions would benefit the accurate predictions for a specific individual [20, 37]. Fourth, our study assumed blood to be a Newtonian fluid. Several cardiovascular studies have compared Newtonian fluid model and non-Newtonian fluid models [10, 49]. Blood flowing at low shear rates should be assumed as a non-Newtonian fluid. However, it has recently been shown that non-Newtonian models, if used, must include appropriate limits otherwise non-Newtonian effects may be overestimated [37]. For example, estimations of viscosity at lower/higher shear rates are often achieved by extrapolation of data below/above the shear rates used to measure rheological properties, which may not reflect the actual rheology of blood. An actual limit exists because there is a physical limit to the shear thinning (and 'thickening') for the viscosity of blood [50]; extrapolation outside such bounds must be interpreted with caution when implementing such values for non-Newtonian blood viscosity into computational models. This study did not calculate the oscillatory shear index (OSI) which indicates the region where potentially lesions initiate and substantially develop. It should be considered in future studies, particularly when such models use fluid-structure interaction in simulations [51]. Regardless of the above limitations, our study demonstrates the potential for added value which can be provided by numerical models in informing clinical practice. A challenge which remains for any models generated with the intention to inform clinical practice is to be able to generated in a timeframe commensurate with diagnostic tests [20, 52].

In this present study we did not consider the vessel wall as flexible tube. It was assumed to be an inelastic wall. It is feasible to include such physical behavior by using fluid-structure interaction [53], which has been previously used to model components of the cardiovascular system [51]. One of the issues, though, with any patient-specific fluid-structure interaction model is the lack of patient-specific data on material properties of the tissue [20]. Therefore, stochastic methods might be necessary for tissue modelling [54] but this introduces variability into predictions. In terms of rheological comparisons for an individual, a model which focuses only on the use of CFD is not expected to alter the qualitative conclusions obtained. Thus, evaluation of the blood flow patterns at stenotic and post-stenotic regions of a blood vessel, based on a transient model, is particularly useful, especially when assessing changes to blood rheology. The concepts outlined in this study can clearly be applied to computational modelling focused on the evaluation of the efficacy of medical devices such as stenting and thrombectomy aspiration device [55, 56].

CONCLUSIONS

Blood flow and wall shear stress in the internal and external carotid arteries are affected differently by pre-bifurcation stenosis. High blood flow velocity presented towards the inner wall of inner carotid artery, which was of consequence to the high WSS at the inner wall in the early systolic phase. Furthermore, hyperglycaemia, increased blood viscosity due to high blood glucose, increases the wall shear stress along a stenosed carotid artery and may particularly affect the blood-flow velocity profile in the external carotid artery (reducing the velocity ratio by as much as ×4). Therefore, this study demonstrates the principle that MRA can be combined with CFD to make predictions for such complicated clinical cases; thus, it opens to a potential for a wider clinical implication.

ACKNOWLEDGMENTS

Johann Guimaraes de Oliverira Marinho was funded as a Science Without Borders exchange student through the CNPQ Foundation during the later parts of this study. Surapong Chatpun was supported by the Faculty of Medicine, Prince of Songkla University (grant number 56-113-25-2-3) and National Science and Technology Development Agency (grant number SCH-NR 2012-181). Furthermore, we would like to thank Ms. Arpapan Prakobkarn and Mr. Natee Ina for MRI acquisition and the volunteer for participation.

REFERENCES

[1] "World Health Organisation." http://www.who.int/mediacentre/factsheets/fs310/en/ (accessed Apr. 01, 2019).

[2] C. A. Holmstedt, T. N. Turan, and M. I. Chimowitz, "Atherosclerotic intracranial arterial stenosis: risk factors, diagnosis, and treatment," *Lancet Neurol.*, vol. 12, no. 11, pp. 1106–1114, 2013, doi: 10.1016/S1474-4422(13)70195-9.

[3] A. M. Johri *et al.*, "Carotid Ultrasound Maximum Plaque Height-A Sensitive Imaging Biomarker for the Assessment of Significant Coronary Artery Disease," *Echocardiography*, vol. 33, no. 2, pp. 281–289, 2016, doi: 10.1111/echo.13007.

[4] J. Pelz, A. Weinreich, D. Fritzsch, and D. Saur, "Quantification of Internal Carotid Artery Stenosis with 3D Ultrasound Angiography," *Ultraschall der Medizin - Eur. J. Ultrasound*, vol. 36, no. 05, pp. 487–493, 2015, doi: 10.1055/s-0034-1398749.

[5] M. Dabagh, P. Vasava, and P. Jalali, "Effects of severity and location of stenosis on the hemodynamics in human aorta and its branches," *Med. Biol. Eng. Comput.*, vol. 53, no. 5, pp. 463–476, 2015, doi: 10.1007/s11517-015-1253-3.

[6] T. Blaser, K. Hofmann, T. Buerger, O. Effenberger, C.-W. Wallesch, and M. Goertler, "Risk of Stroke, Transient Ischemic Attack, and Vessel Occlusion Before Endarterectomy in Patients With Symptomatic Severe Carotid Stenosis," *Stroke*, vol. 33, no. 4, pp. 1057–1062, 2002, doi: 10.1161/01.STR.0000013671.70986.39.

[7] P. M. Rothwell and C. P. Warlow, "Low Risk of Ischemic Stroke in Patients With Reduced Internal Carotid Artery Lumen Diameter Distal to Severe Symptomatic Carotid Stenosis," *Stroke*, vol. 31, no. 3, pp. 622–630, 2000, doi: 10.1161/01.STR.31.3.622.

[8] Z.-Y. Li, F. P. P. Tan, G. Soloperto, N. B. Wood, X. Y. Xu, and J. H. Gillard, "Flow pattern analysis in a highly stenotic patient-specific carotid bifurcation model using a turbulence model," *Comput. Methods Biomech. Biomed. Engin.*, vol. 18, no. 10, pp. 1099–1107, 2015, doi: 10.1080/10255842.2013.873033.

[9] A. Millon *et al.*, "Low WSS Induces Intimal Thickening, while Large WSS Variation and Inflammation Induce Medial Thinning, in an Animal Model of Atherosclerosis," *PLoS One*, vol. 10, no. 11, p. e0141880, 2015, doi: 10.1371/journal.pone.0141880.

[10] A. Razavi, E. Shirani, and M. R. Sadeghi, "Numerical simulation of blood pulsatile flow in a stenosed carotid artery using different rheological models," *J. Biomech.*, vol. 44, no. 11, pp. 2021–2030, 2011, doi: 10.1016/j.jbiomech.2011.04.023.

[11] P. Siogkas *et al.*, "Multiscale - Patient-Specific Artery and Atherogenesis Models," *IEEE Trans. Biomed. Eng.*, vol. 58, no. 12, pp. 3464–3468, 2011, doi: 10.1109/TBME.2011.2164919.

[12] B. Sui, P. Gao, Y. Lin, L. Jing, S. Sun, and H. Qin, "Hemodynamic parameters distribution of upstream, stenosis center, and downstream sides of plaques in carotid artery with different stenosis: a MRI and CFD study," *Acta radiol.*, vol. 56, no. 3, pp. 347–354, 2015, doi: 10.1177/0284185114526713.

[13] Y. A. Algabri, S. Rookkapan, V. Gramigna, D. M. Espino, and S. Chatpun, "Computational study on hemodynamic changes in patient-specific proximal neck angulation of abdominal aortic aneurysm with time-varying velocity," *Australas. Phys. Eng. Sci. Med.*, vol. 42, no. 1, pp. 181–190, 2019, doi: 10.1007/s13246-019-00728-7.

[14] C. Karmonik *et al.*, "Quantitative comparison of hemodynamic parameters from steady and transient CFD simulations in cerebral aneurysms with focus on the aneurysm ostium," *J. Neurointerv. Surg.*, vol. 7, no. 5, pp. 367–372, 2015, doi: 10.1136/neurintsurg-2014-011182.

[15] J. V. Lassaline and B. C. Moon, "A computational fluid dynamics simulation study of coronary blood flow affected by graft placement," *Interact. Cardiovasc. Thorac. Surg.*, vol. 19, no. 1, pp. 16–20, 2014, doi: 10.1093/icvts/ivu034.

[16] S. Mei, F. S. N. de Souza Júnior, M. Y. S. Kuan, N. C. Green, and D. M. Espino, "Hemodynamics through the congenitally bicuspid aortic valve: a computational fluid dynamics comparison of opening orifice area and leaflet orientation," *Perfusion*, vol. 31, no. 8, pp. 683–690, 2016, doi: 10.1177/0267659116656775.

[17] S. M. A. Khader, B. S. Shenoy, R. Pai, S. G. Kamath, N. M. Sharif, and V. R. K. Rao, "Effect of increased severity in patient specific stenosis of common carotid artery using CFD-a case study," *World J. Model. Simul.*, vol. 7, pp. 113–122, 2011.

[18] C. Öhman, D. M. Espino, T. Heinmann, M. Baleani, H. Delingette, and M. Viceconti, "Subject-specific knee joint model: Design of an experiment to validate a multi-body finite element model," *Vis. Comput.*, vol. 27, no. 2, pp. 153–159, 2011, doi: 10.1007/s00371-010-0537-8.

[19] H. Bahraseman *et al.*, "Combining numerical and clinical methods to assess aortic valve hemodynamics during exercise," *Perfusion*, vol. 29, no. 4, pp. 340–350, 2014, doi: 10.1177/0267659114521103.

[20] H. G. Bahraseman, K. Hassani, M. Navidbakhsh, D. M. Espino, Z. A. Sani, and N. Fatouraee, "Effect of exercise on blood flow through the aortic valve: a combined clinical and numerical study," *Comput. Methods Biomech. Biomed. Engin.*, vol. 17, no. 16, pp. 1821–1834, 2014, doi: 10.1080/10255842.2013.771179.

[21] D. A. Steinman, J. B. Thomas, H. M. Ladak, J. S. Milner, B. K. Rutt, and J. D. Spence, "Reconstruction of carotid bifurcation hemodynamics and wall thickness using computational fluid dynamics and MRI," *Magn. Reson. Med.*, vol. 47, no. 1, pp. 149–159, 2002, doi: 10.1002/mrm.10025.

[22] H. E. Burton, R. Cullinan, K. Jiang, and D. M. Espino, "Multiscale three-dimensional surface reconstruction and surface roughness of porcine left anterior descending coronary arteries," *R. Soc. Open Sci.*, vol. 6, no. 9, p. 190915, 2019, doi: 10.1098/rsos.190915.

[23] N. Antonova, X. Dong, P. Tosheva, E. Kaliviotis, and I. Velcheva, "Numerical analysis of 3D blood flow and common carotid artery hemodynamics in the carotid artery bifurcation with stenosis," *Clin. Hemorheol. Microcirc.*, vol. 57, no. 2, pp. 159–173, 2014, doi: 10.3233/CH-141827.

[24] D. Gallo, D. A. Steinman, and U. Morbiducci, "An Insight into the Mechanistic Role of the Common Carotid Artery on the Hemodynamics at the Carotid Bifurcation," *Ann. Biomed. Eng.*, vol. 43, no. 1, pp. 68–81, 2015, doi: 10.1007/s10439-014-1119-0.

[25] Y. I. Cho, M. P. Mooney, and D. J. Cho, "Hemorheological Disorders in Diabetes Mellitus," *J. Diabetes Sci. Technol.*, vol. 2, no. 6, pp. 1130–1138, 2008, doi: 10.1177/193229680800200622.

[26] D. A. Fedosov, M. Dao, G. E. Karniadakis, and S. Suresh, "Computational Biorheology of Human Blood Flow in Health and Disease," *Ann. Biomed. Eng.*, vol. 42, no. 2, pp. 368–387, 2014, doi: 10.1007/s10439-013-0922-3.

[27] A. Prakobkarn, S. Chatpun, N. Ina, S. Saeheng, and N. Chantarapanich, "Influences of vascular geometry and blood property on carotid artery hemodynamics," 2013, doi: 10.1109/BMEiCon.2013.6687731.

[28] P. Goswami, D. K. Mandal, N. K. Manna, and S. Chakrabarti, "Numerical investigations of various aspects of plaque deposition through constricted artery," *J. Mech. Eng. Sci.*, vol. 13, no. 3, pp. 5306–5322, 2019, doi: 10.15282/jmes.13.3.2019.07.0433.

[29] R. S. and W. S. C. Caro, T. Pedley, *The Mechanics of the Circulation*. Cambridge, UK: Cambridge University Press, 2012.

[30] J. De Hart, G. W. M. Peters, P. J. G. Schreurs, and F. P. T. Baaijens, "A two-dimensional fluid–structure interaction model of the aortic value," *J. Biomech.*, vol. 33, no. 9, pp. 1079–1088, 2000, doi: 10.1016/S0021-9290(00)00068-3.

[31] M. Y. S. Kuan and D. M. Espino, "Systolic fluid–structure interaction model of the congenitally bicuspid aortic valve: assessment of modelling requirements," *Comput. Methods Biomech. Biomed. Engin.*, vol. 18, no. 12, pp. 1305–1320, 2015, doi: 10.1080/10255842.2014.900663.

[32] J. Vekasi, Z. S. Marton, G. Kesmarky, A. Cser, R. Russai, and B. Horvath, "Hemorheological alterations in patients with diabetic retinopathy," *Clin Hemorheol Microcirc*, vol. 24, no. 1, pp. 59–64, 2001.

[33] N. Filipovic and M. Kojic, "Computer simulations of blood flow with mass transport through the carotid artery bifurcation," *Theor. Appl. Mech.*, vol. 31, no. 1, pp. 1–33, 2004, doi: 10.2298/TAM0401001F.

[34] M. E. Wagshul, P. K. Eide, and J. R. Madsen, "The pulsating brain: A review of experimental and clinical studies of intracranial pulsatility," *Fluids Barriers CNS*, vol. 8, no. 1, p. 5, 2011, doi: 10.1186/2045-8118-8-5.

[35] M. L. Bots, "Low diastolic blood pressure and atherosclerosis in elderly subjects. The Rotterdam study," *Arch. Intern. Med.*, vol. 156, no. 8, pp. 843–848, 1996, doi: 10.1001/archinte.156.8.843.

[36] Y. Hoi, B. A. Wasserman, E. G. Lakatta, and D. A. Steinman, "Carotid Bifurcation Hemodynamics in Older Adults: Effect of Measured Versus Assumed Flow Waveform," *J. Biomech. Eng.*, vol. 132, no. 7, p. 071006, 2010, doi: 10.1115/1.4001265.

[37] G. Carty, S. Chatpun, and D. M. Espino, "Modeling Blood Flow Through Intracranial Aneurysms: A Comparison of Newtonian and Non-Newtonian Viscosity," *J. Med. Biol. Eng.*, vol. 36, no. 3, pp. 396–409, 2016, doi: 10.1007/s40846-016-0142-z.

[38] D. Katritsis, L. Kaiktsis, A. Chaniotis, J. Pantos, E. P. Efstathopoulos, and V. Marmarelis, "Wall Shear Stress: Theoretical Considerations and Methods of Measurement," *Prog. Cardiovasc. Dis.*, vol. 49, no. 5, pp. 307–329, 2007, doi: 10.1016/j.pcad.2006.11.001.

[39] A. Prakobkarn, N. Ina, S. Saeheng, and S. Chatpun, "Carotid artery stenosis pre-assessment by relationship derived from two-dimensional patient-specific model and throat velocity ratio," *World J. Model. Simul.*, vol. 13, pp. 3–11, 2017.

[40] S. E. Lee, S.-W. Lee, P. F. Fischer, H. S. Bassiouny, and F. Loth, "Direct numerical simulation of transitional flow in a stenosed carotid bifurcation," *J. Biomech.*, vol. 41, no. 11, pp. 2551–2561, 2008, doi: 10.1016/j.jbiomech.2008.03.038.

[41] M. Markl *et al.*, "In Vivo Wall Shear Stress Distribution in the Carotid Artery," *Circ. Cardiovasc. Imaging*, vol. 3, no. 6, pp. 647–655, 2010, doi: 10.1161/CIRCIMAGING.110.958504.

[42] H. Gharahi, B. A. Zambrano, D. C. Zhu, J. K. DeMarco, and S. Baek, "Computational fluid dynamic simulation of human carotid artery bifurcation based on anatomy and volumetric blood flow rate measured with magnetic resonance imaging," *Int. J. Adv. Eng. Sci. Appl. Math.*, vol. 8, no. 1, pp. 46–60, 2016, doi: 10.1007/s12572-016-0161-6.

[43] S. S. Varghese, S. H. Frankel, and P. F. Fischer, "Direct numerical simulation of stenotic flows. Part 2. Pulsatile flow," *J. Fluid Mech.*, vol. 582, p. 281, 2007, doi: 10.1017/S0022112007005836.

[44] D. N. Ku, D. P. Giddens, C. K. Zarins, S. Glagov, and M. A. Y. June, "Pulsatile Flow and Atherosclerosis in the Human Carotid Bifurcation," *Ateriosclerosis*, vol. 5, no. 3, pp. 293–302, 1985.

[45] Q. Long, X. . Xu, K. . Ramnarine, and P. Hoskins, "Numerical investigation of physiologically realistic pulsatile flow through arterial stenosis," *J. Biomech.*, vol. 34, no. 10, pp. 1229–1242, 2001, doi: 10.1016/S0021-9290(01)00100-2.

[46] H. G. Bahraseman, E. M. Languri, N. Yahyapourjalaly, and D. M. Espino, "Fluid–structure interaction modeling of aortic valve stenosis at different heart rates," *Acta Bioeng. Biomech.*, vol. 18, no. 3, pp. 11–20, 2016, doi: 10.5277/ABB-00429-2015-03.

[47] H. E. Burton, J. M. Freij, and D. M. Espino, "Dynamic Viscoelasticity and Surface Properties of Porcine Left Anterior Descending Coronary Arteries," *Cardiovasc. Eng. Technol.*, vol. 8, no. 1, pp. 41–56, 2017, doi: 10.1007/s13239-016-0288-4.

[48] J. M. Freij, H. E. Burton, and D. M. Espino, "Objective Uniaxial Identification of Transition Points in Non-Linear Materials: Sample Application to Porcine Coronary Arteries and the Dependency of Their Pre- and Post-Transitional Moduli with Position," *Cardiovasc. Eng. Technol.*, vol. 10, no. 1, pp. 61–68, 2019, doi: 10.1007/s13239-018-00395-x.

[49] B. Chen, T. Lambrou, A. C. Offiah, P. A. Gondim Teixeira, M. Fry, and A. Todd-Pokropek, "An in vivo subject-specific 3D functional knee joint model using combined MR imaging," *Int. J. Comput. Assist. Radiol. Surg.*, vol. 8, no. 5, pp. 741–750, 2013, doi: 10.1007/s11548-012-0801-7.

[50] S. Chatpun and P. Cabrales, "Effects of plasma viscosity modulation on cardiac function during moderate hemodilution," *Asian J. Transfus. Sci.*, vol. 4, no. 2, p. 102, 2010, doi: 10.4103/0973-6247.67034.

[51] D. M. Espino, D. E. T. Shepherd, and D. W. L. Hukins, "Evaluation of a transient, simultaneous, arbitrary Lagrange–Euler based multi-physics method for simulating the mitral heart valve," *Comput. Methods Biomech. Biomed. Engin.*, vol. 17, no. 4, pp. 450–458, 2014, doi: 10.1080/10255842.2012.688818.

[52] C. E. Lavecchia *et al.*, "Lumbar model generator: a tool for the automated generation of a parametric scalable model of the lumbar spine," *J. R. Soc. Interface*, vol. 15, no. 138, p. 20170829, 2018, doi: 10.1098/rsif.2017.0829.

[53] D. M. Espino, D. E. T. Shepherd, and D. W. L. Hukins, "Transient large strain contact modelling: A comparison of contact techniques for simultaneous fluid–structure interaction," *Eur. J. Mech. - B/Fluids*, vol. 51, pp. 54–60, 2015, doi: 10.1016/j.euromechflu.2015.01.006.

[54] D. M. Espino, J. R. Meakin, D. W. L. Hukins, and J. E. Reid, "Stochastic Finite Element Analysis of Biological Systems: Comparison of a Simple Intervertebral Disc Model with Experimental Results," *Comput. Methods Biomech. Biomed. Engin.*, vol. 6, no. 4, pp. 243–248, 2003, doi: 10.1080/10255840310001606071.

[55] C. Talayero, G. Romero, G. Pearce, and J. Wong, "Thrombectomy aspiration device geometry optimization for removal of blood clots in cerebral vessels," *J. Mech. Eng. Sci.*, vol. 14, no. 1, pp. 6229–6237, 2020, doi: 10.15282/jmes.14.1.2020.02.0487.

[56] G. Romero, C. Talayero, G. Pearce, and J. Wong, "Modeling of blood clot removal with aspiration Thrombectomy devices," *J. Mech. Eng. Sci.*, vol. 14, no. 1, pp. 6238–6250, 2020, doi: 10.15282/jmes.14.1.2020.03.0488.